Numerical simulation of ramp induced shock wave/boundary-layer interaction in turbulent flow

Asmelash H. A.
ahaftu@yahoo.com, asmilh@gmail.com
Aeronautical Engineering Department, Defence University
College of Engineering
Ethiopia

R. R. Martis
Department of Aerospace Engineering
Defence Institute of Advanced Technology
India

A. Singh
Terminal Ballistics Research Laboratory (TBRL)
Chandigarh
India

ABSTRACT

A computational study has been carried out to analyse the shock wave turbulent boundary layer interaction in a two-dimensional compression ramp flow for a free stream Mach number of 2·94. Ramp angles ranging from 8° to 24° are used to produce the full range of possible flow fields, including flows with minor separation, moderate separation, and significant amount of separation. The model has been analysed using 2D numerical simulations based on a commercially available Computational Fluid Dynamics (CFD) Code, Fluent, that employs k-ω Shear Stress Transport (SST) turbulence model. The computed data for surface pressure distribution indicated a good agreement with experiment. Numerical results obtained through the present series of computations indicate an increased extent of separated zone, and thus show increased upstream influence when compared to experiment. Total pressure loss has shown to increase downstream of separation location and increase when corner angle increases. Secondary separation has been observed for higher angles.

Paper No. 3742. Manuscript received 21 July 2011, revised version received 16 March 2012, 2nd revised version received 11 October 2012, accepted 15 November 2012.

https://doi.org/10.1017/S0001924000008253 Published online by Cambridge University Press

NOMENCLATURE

O	interaction origin
C	shock wave
CFD	Computational Fluid Dynamics
M_∞	upstream Mach number
RANS	Reynolds Averaged Navier-Stokes equations
R	reattachment location
S	separation location
SST	Shear Stress Transport
SWTBLI	Shock Wave Turbulent Boundary-Layer Interaction
T_0, P_0	total temperature, total pressure
δ	boundary-layer thickness

1.0 INTRODUCTION

The interaction between a shock wave and a boundary layer (SWBLI) is one of the most challenging problems of modern high speed fluid dynamics. The complicated nature of the separated boundary-layer, due to the interaction, embodies unfavourable effects such as fluctuating pressure and heat transfer loads, and changes in flow topology which results in non-uniformity of the flow-field. These interactions are prevalent in a variety of high speed applications such as long haul civil transportation systems as well as military high-speed manoeuvring vehicles. The induced separation on these systems causes loss of control surface effectiveness, loss of total pressure, drop in air intake efficiency and can also cause large scale fluctuations such as detrimental air intake buzz or engine extinction, and buffeting or fluctuating side loads in separated propulsive nozzles. Therefore, an in-depth knowledge of the phenomena is essential for efficiaent aerodynamic and propulsion design.

A ramp interaction occurs when a supersonic flow is deflected by a wedge or a compression corner. The adverse pressure gradient, due to the shock, propagates upstream through the subsonic part of the boundary layer. If this adverse pressure gradient is sufficiently large, so as to overcome its inertia, the boundary layer will separate. A detailed study of the structure of the SWBLI induced due

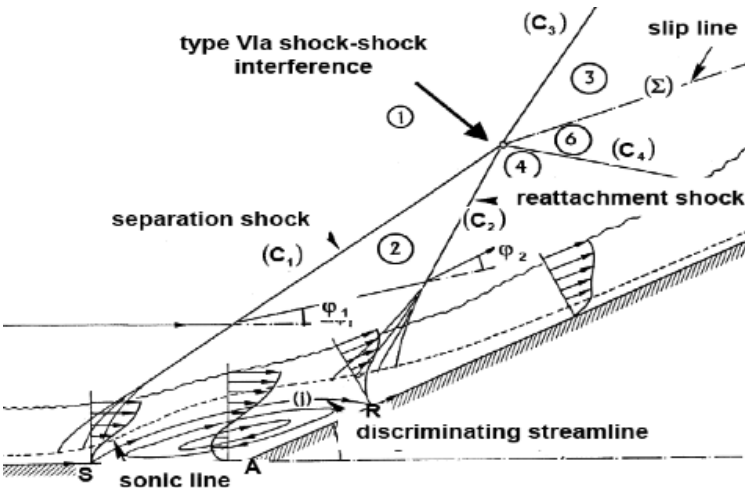


Figure 1. Structure of SWBLI due to a ramp[3].

https://doi.org/10.1017/S0001924000008253 Published online by Cambridge University Press

to a ramp[1] is depicted in Fig. 1. A sufficiently large adverse pressure gradient causes a separation of the boundary layer at point *S* called the separation point. This separation is accompanied by the formation of a separation shock, C_1. The location of reattachment of the separation is indicated at point *R* and the corresponding reattachment shock as C_2. The distance between the corner, *A*, and the location of the initial pressure rise is defined as the upstream influence length. An increase in shock strength increases this upstream influence[2]. Experimental studies on the effect of the nature of the boundary layer[3] revealed that the interaction is essentially the same irrespective of whether the boundary layer is laminar or turbulent. Only the scales of interaction and the intensity of the rise in pressure and skin friction are magnified in the case of turbulent flows. Computations using Reynolds Averaged Navier Stokes equations (RANS)[4] are reasonably accurate for 'weak' interactions but produce poor predictions of skin friction and heat transfer in the case of strong interactions. Also work conducted by Oliver *et al*[4] using OVERFLOW code which employs SST of *k*-ω turbulence model developed by the authors showed more separation than other turbulence models. A delayed reattachment appears to be a source of these discrepancies.

The first objective of this paper is to assess the accuracy of the *k*-ω SST turbulence model for the different ramp angles studied namely 8°, 16°, 20° and 24° at Mach 2·94. The computed flowfield results are compared with the experimental data of references[4,5,6] for surface pressure distribution.

The second objective is an assessment of the separation and reattachment locations based on the shear stress distribution. A qualitative description of the interaction is also presented based on the density contours.

The third objective is the examination of the effect of the interaction on the total pressure in the boundary layer. A comparison of the effect of increasing ramp angle on the boundary-layer total pressure, in the interaction region, is also carried out.

2.0 COMPUTATIONAL SETUP

To study the flow-field of the interaction, the basic ramp flow geometry used in[4,5,6] has been adopted for the present study, primarily due to the availability of experimental data. The experiments made use of a two-component Laser Doppler velocity meter to study the nature of turbulence downstream of the interaction. This method prevented the use of splitter plates to eliminate the sidewall boundary-layer effects. A full span model of the compression ramp was thus used such that the ramp interaction measurements were unaffected by the sidewall boundary-layer effects.

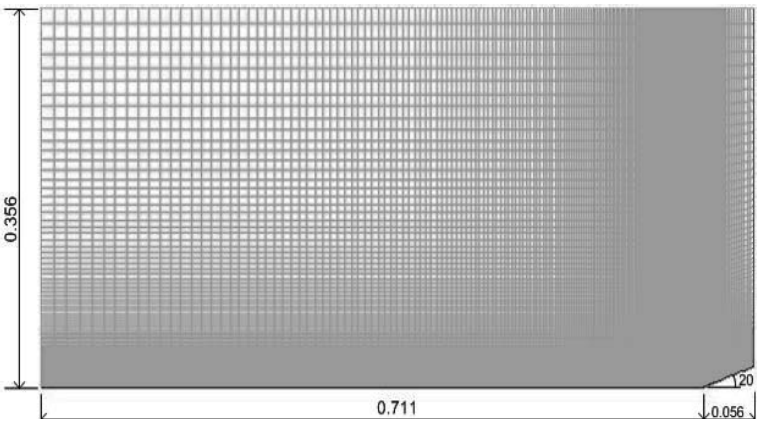


Figure 2. Grid system (computational domain, dimension in meters).

https://doi.org/10.1017/S0001924000008253 Published online by Cambridge University Press

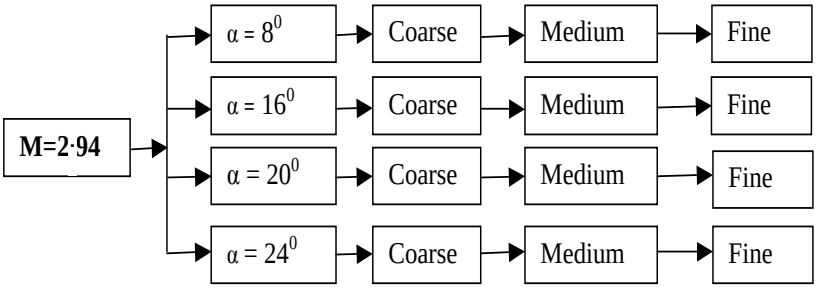


Figure 3. Flowchart of Solution.

The computational domain extends from a prescribed location upstream of the interaction where a turbulent boundary layer is generated, to a point well downstream of the interaction. Domain height is taken large enough so that shock-shock interaction does not reach that height and flow at that height is the free stream flow and is not affected by the interaction taking place near the wall. Basic mesh details of the ramp (20°) are shown in Fig. 2 with a typical grid distribution clustered near the corner region. Upstream extent used is large enough to build up the required turbulent boundary-layer thickness. Computations were made by using grid to grid file interpolation technique in a sequence of progressively finer grids with three different grids [Grid 1 (57,000 cells), Grid 2 (70,000 cells) and Grid 3 (110,000 cells)] in two blocks and $0 < y + < 0{\cdot}35$.

A large upstream extent is defined so that the boundary layer can develop naturally, starting with a zero thickness boundary layer at the leading edge of the plate. At the corner location of the plate (measured in the absence of the compression corner), the boundary-layer thickness reported in the experiment is given to be 8·27mm. The computed boundary-layer thickness in the present study was found to be 9mm which exceeds the experimental value by around 8%. This value is being used for normalising the length and height in the preceding sections.

The initial boundary layer is measured at the location of the corner of the flat plate before the flat plate was turned in to a corner (measured in the absence of the compression corner). This is so because we cannot measure the boundary-layer thickness when there is a corner as the region is separated afterwards.

A commercially available CFD code, Fluent, has been used to simulate the different configurations. A density based steady, implicit solver with upwind second order discretisation scheme for flow and transport equations was chosen to capture shocks better at cell faces. Turbulence is solved using the SST k-ω[7] turbulence model. Convergence criteria were considered when residuals fell by three orders and the measurement of shear stress at three different locations (upstream, within and downstream of the separation zone) converged to four significant digits. A converged solution was obtained between 50,000-60,000 iterations.

Table1
Inlet boundary conditions

S/N	Ramp [degree]	M_∞	T_0 [K]	P_0 [Pa]	Re_∞ [m^{-1}]
1	8°	2·94	294	4·83e + 05	$36{\cdot}4 \times 10^6$
2	16°	2·94	303	4·83e + 05	$36{\cdot}4 \times 10^6$
3	20°	2·94	303	4·83e + 05	$36{\cdot}4 \times 10^6$
4	24°	2·94	302	4·83e + 05	$36{\cdot}4 \times 10^6$

https://doi.org/10.1017/S0001924000008253 Published online by Cambridge University Press

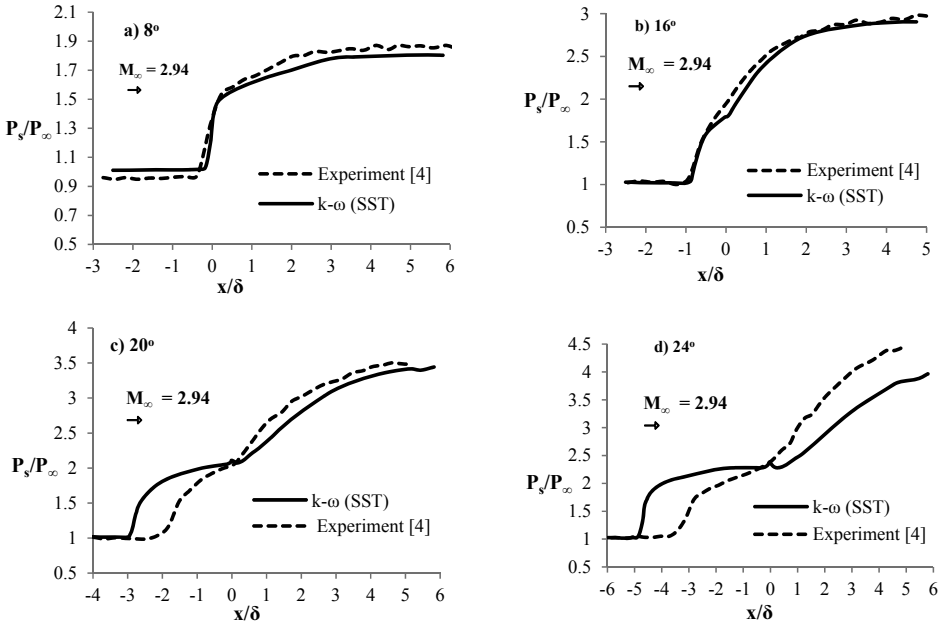


Figure 4. Computed and experimental results for the pressure ratio.

The boundary conditions at the inlet, for the different configurations, are presented in Table 1. These conditions are the same as the experimental test conditions[4,5,6]. The outlet is specified as a supersonic outlet. Adiabatic, no slip boundary condition is imposed on all the walls. A zero normal gradient is specified on the boundary opposite the walls. A turbulence intensity of 5% and turbulent viscosity ratio of 5 has been used. In the turbulence category, Turbulent Viscosity Ratio is the ratio of turbulent viscosity to the laminar viscosity and Turbulence Intensity is the ratio of the magnitude of the Root Mean Square (RMS) turbulent fluctuations to the reference velocity (the mean velocity magnitude for the flow). Boundary-layer thickness (δ) measured from the experiments[4,5,6] was 8·27mm.

3.0 RESULTS AND DISCUSSIONS

3.1 Validation of turbulence model

Figure 4 shows the ratio of wall static pressure to free stream static pressure comparison of the computed and experimental results for the different ramp deflection angles studied. The pressure and *x*-location are normalised using the inlet static pressure of 14,391Pa and the boundary-layer thickness of 9mm, respectively. For the weak interactions (Figs 4(a) and (b)) the numerical results show the same trend as the experimental results. For the 8° ramp angle case, a shift in the pressure ratios is observed upstream and downstream of the interaction. This characteristic was observed by earlier studies using the OVERFLOW code with SST turbulence model as well(4). The reason for this discrepancy is attributed to a possible error in the experimental measurement for this configuration. Hence, the deviation in the location of initial pressure rise for the 8° ramp

https://doi.org/10.1017/S0001924000008253 Published online by Cambridge University Press

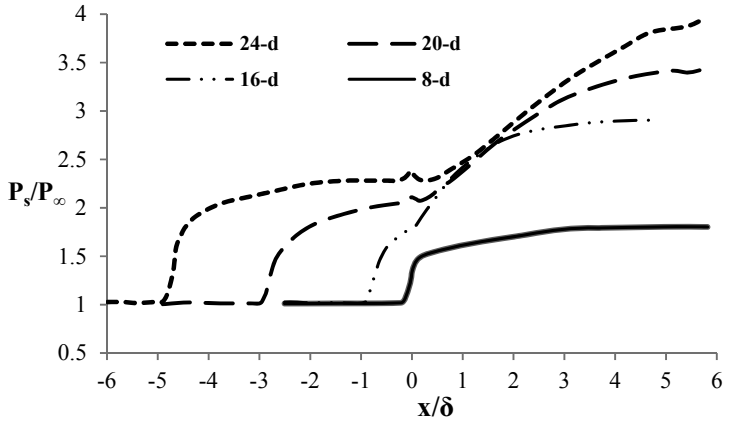


Figure 5. Comparison of surface static pressure distributions for 8°-24° ramps.

angle varies by around 41%. The computations for the interaction involving the 16° ramp is in very good agreement with the experimental data throughout the interaction region and the variation at the location of the initial pressure rise is around 3·5%. With increasing shock strength (20° and 24°), the numerical results show larger upstream influence (Figs 4(c) and (d)) in comparison with the experimental results. This deviation from experiments is 36% and 43% in the case of the ramp angles of 20° and 24°, respectively. The reason is that, the turbulence model itself is not accurately modelling the flow physics of the problem when interaction strength increases.

Figure 5 shows the comparison of surface static pressure distribution for the ramp angles studied. Following the initial rise in pressure from the upstream influence location, the nature of the pressure distribution in the 8° ramp angle case is similar to the experimental results. As reported in earlier studies[4,5,6], no plateau is observed in the 8° corner flow. However, an examination of the velocity vector contours, as shown in Fig. 6, reveals a small reversed flow region indicating a very small separation bubble. The size of this bubble is negligibly small so that it

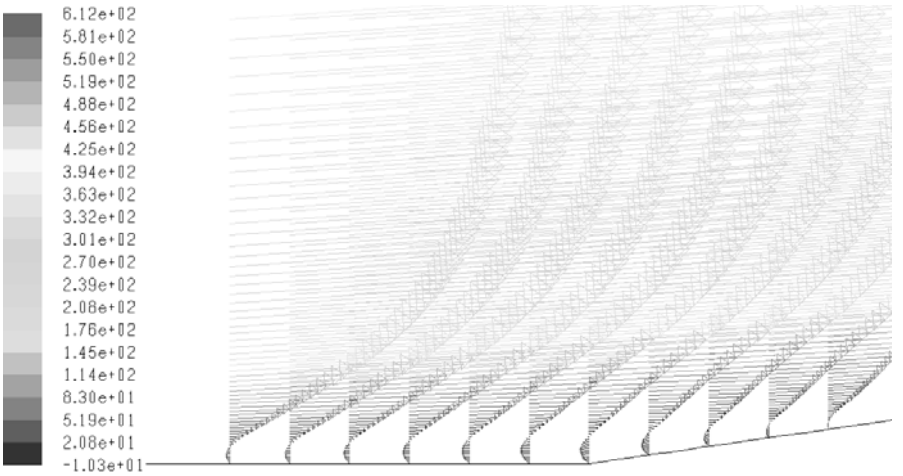


Figure 6. Velocity vector near the corner region for 8° ramp flow at M = 2·94.

https://doi.org/10.1017/S0001924000008253 Published online by Cambridge University Press

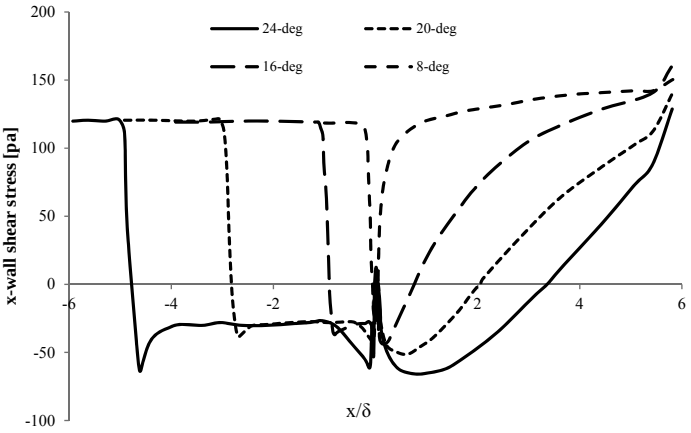


Figure 7. Wall Shear Stress distribution for ramp angles.

does not create any radical change of the flow characteristics. However, the separation cannot be ignored easily as there is 10·3ms^{-1} of velocity in the reverse direction which amounts up to about 1·7%. With increasing shock strength, a plateau region is observed after an initial rise in pressure, indicating a clear separation of the flow. The start of the plateau region indicates the separation point and the end of the plateau indicates the location where the crest of the bubble is situated. The size of the plateau increases with increasing shock strength. Thereafter, an increase in pressure is observed towards the reattachment location. In the strongest cases studied (20° and 24°), a small kink in the pressure distribution is observed between the plateau and the peak pressure regions. This kink is suggestive of a secondary separation within the separation bubble and will be discussed subsequently.

3.2 Assessment of separation and reattachment locations

Figure 7 shows the wall shear stress distribution for the different ramp angles studied. For the weakest interaction, a sharp drop in the wall shear stress is observed close to the corner location leading to a small negative value. Negative shear stress signifies negative velocity gradients associated with the reversed (negative) velocity in the separation bubble. This negative shear stress strengthens the observation of separation in the 8° ramp configuration studied. The separation length of the interaction is very small in this case which can be concluded from the zeros of the function indicating the separation and reattachment point.

With increasing shock strength, the length to which the adverse pressure gradient is propagated upstream increases. The magnitude of the negative shear stress also increases as seen in Fig. 7. In the case of the 20° and 24° ramps, a kink in the skin friction distribution is observed near the ramp corner which signifies another separation zone (Fig. 8). This kink represents a secondary separation. Previous studies[4,8] of the same ramp angles at Mach 2·85 did not show any such feature. To the knowledge of the authors, this is the first observation of its kind. The kink was not observed in the experiment. While experiments can be taken as a bench mark because of their reliability, the measurements are restricted to the discrete probe locations. Experiments thus have shortcomings in that they do not analyse every point in the flow domain. The CFD analysis presented warrants the need for additional experiments. This secondary separation at the corner of the ramp is also clearly indicated in the velocity vector contour as shown in Fig. 9 for the 24° ramp.

https://doi.org/10.1017/S0001924000008253 Published online by Cambridge University Press

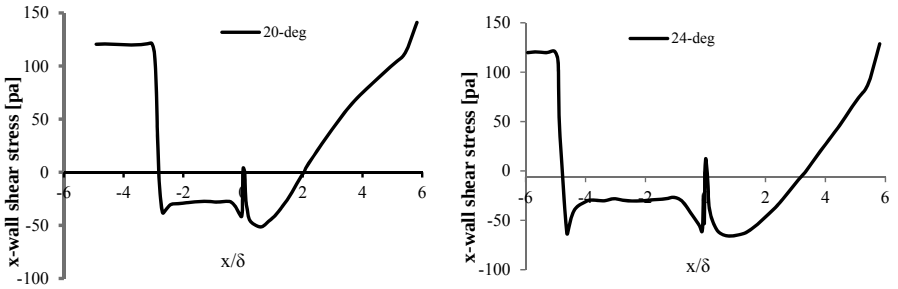


Figure 8. Wall shear stress distributions at ramp angles of 20° and 24°.

Figure 9 provides a qualitative description of the flow highlighting secondary separation. Figure 9 is magnified for clarity and is not for quantitative analysis. Separation causes a reversal in flow direction. Fig. 9 clearly shows secondary separation near the corner region. The free-stream flow is directed from left to right (→) in the computational domain. For a largely separated flow field (like in 24° compression corner) the stronger adverse pressure gradient (in the corner region) causes the velocity field to be reversed and directed towards the left (right to left, ←,). Within this separated region, an additional reversal of flow is observed, directed towards the right (left to right, →,) near the corner. This region is the secondary separation region. This fact is verified both with velocity vector (Fig. 9) and shear stress (Fig. 8) plots but is small in magnitude.

Figure 10, gives the density contours for the different ramp configurations studied. At 8°, the flow appears to be attached. The separation bubble, as discussed in earlier sections, is very small and does not show up in the density contour. The shock appears to originate at the corner location and the curvature of the shock results from Mach number gradient in the incoming boundary layer. A significant upstream influence is seen for the 16° ramp, showing the clear evidence of separation. The 20° and 24° corner angles show a stronger upstream influence. For 20° and 24° ramps, a second shock is observed downstream of the separation shock. This second shock is the reattachment shock. The intersection of separation and reattachment shocks indicates a slight bend from which a stronger shock appears due to merging of the two left running shocks. This phenomenon is similar to the commonly known shock-shock interaction due to two left running shocks also called the type VI shock-shock interaction.

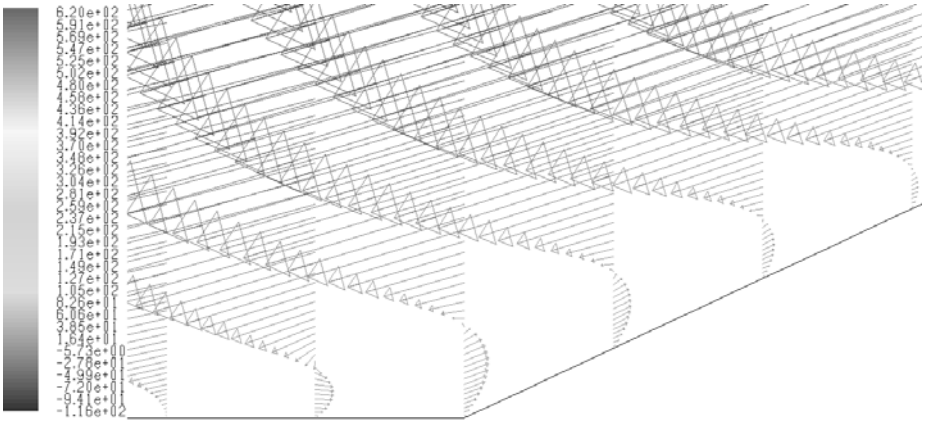


Figure 9. Velocity vector inside the separated region for 24° ramp flow at M = 2·94.

https://doi.org/10.1017/S0001924000008253 Published online by Cambridge University Press

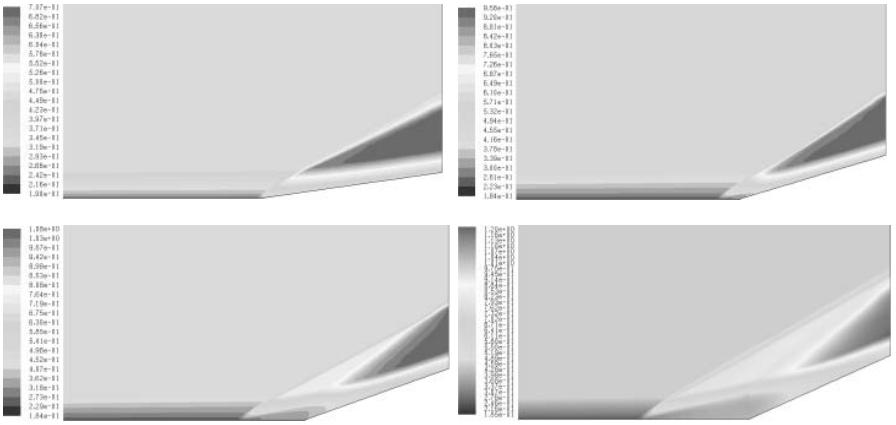


Figure 10. Density contours near the corner regions (8°, 16°, 20° and 24°).

3.3 Effect of interaction on total pressure in the boundary layer

Figure 11 gives the total pressure ratio profiles, in the boundary layer, for the different angles at the ramp corner, 'x = 0 mm'. For the 20° and 24° ramp interactions, a larger loss is observed in the boundary-layer region closer to the wall. The reason is that the stronger interaction causing the primary separation induces larger loss of total pressure in the separated region. Also, the larger loss could be due to the secondary separation discussed in Section 3.2. It is observed that at a given height, y = 5 mm, the loss in total pressure increases with increasing deflection angle due to the increase in shock strength and increased separation. The occurrence of such a phenomenon would, therefore, reduce the efficiency of the system.

In Figure 12, a comparison of total pressure loss is presented for the 24° ramp. The behaviour of the boundary layer due to the interaction induced by the smaller ramp angles is similar to the 24° ramp but to a smaller extent. Here, only the strongest case is considered. The total pressure is measured at four different locations of the interaction namely; at the separation location '*S*', at ramp corner '0', at the reattachment location '*R*' and, at a location 4δ downstream of the ramp corner which is also downstream of the reattachment point. The total pressure loss inside the boundary layer is observed to be maximum at the corner location. For a given total pressure the height y increases with location downstream of the separation point, consistent with an increase in boundary-layer thickness with stream-wise distance. This is because the magnitude of total pressure depends on static pressure which increases downstream and the effect of the separation is carried downstream of the interaction. Due to these losses, the boundary layer requires a larger

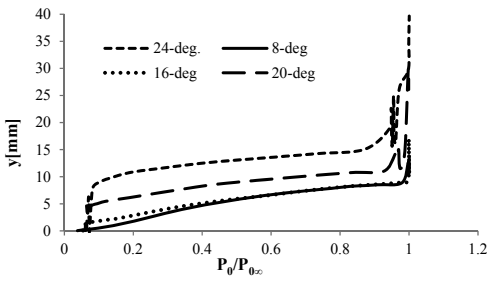


Figure 11. Total pressure ratios 8°-24° at ramp corner, x = 0mm.

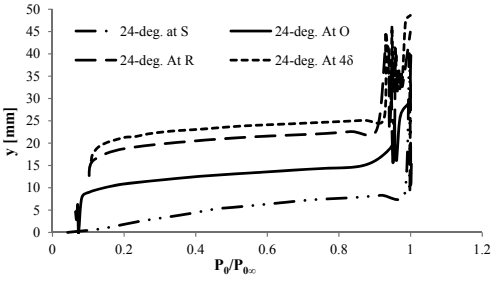


Figure 12. Total pressure ratios at *S, O, R* and 4δ-locations for 24° ramp.

https://doi.org/10.1017/S0001924000008253 Published online by Cambridge University Press

length, downstream of the interaction, to recover. Even at the 4δ location downstream of the corner, the boundary layer has not recovered. The effect of the interaction persists even after the reattachment of the boundary layer.

CONCLUSIONS

The predictions of the shock wave turbulent boundary-layer interaction, induced by a ramp, using SST *k-ω turbulence model,* are compared with experimental results. Moderate to significant discrepancies occur in the strong and very strong interactions. The data curves for the computed and experimental pressure ratios (Figs 4(c) and 4(d)), of strong interactions, show over prediction at separation and under prediction at reattachment locations. The stronger the interaction, the more the numerical solutions deviates from experimental results since, the turbulence model itself is not accurately modelling the flow physics of the problem for stronger interactions. This is the limitation of the turbulence model.

Separation is observed even for the smallest angle studied. This separation shows up in the reversal of velocity vectors in the contours but is very small and does not cause any drastic changes in the flow features.

The wall shear stress distributions indicate a secondary separation for the strong interaction caused by the 20° and 24° ramps. This secondary separation is observed in the immediate vicinity of the ramp corner.

The total pressure losses in the boundary-layer increase with increasing shock strength. The effect of boundary-layer separation persists downstream of reattachment. For the 24° ramp, even 4δ downstream of the corner, the boundary layer is observed to have not recovered to its original profile.

ACKNOWLEDGEMENT

The authors are sincerely thankful to Defence University, College of Engineering, Bishoftu, Ethiopia; Defence Institute of Advanced Technology, Girinagar, Pune; and Terminal Ballistics Research Laboratory, Chandigarh, India, for supporting this work.

REFERENCES

1. J.M. DELERY. Shock Wave Turbulent Boundary Layer Interaction and its Control, *Aerospace Sci*, 1985, **22**, pp 209-280.
2. SETTLES, G.S., FITZPATRICK, T.J. and BOGDONOFF, S.M. A detailed study of attached and separated compression corner flow-fields in high Reynolds number supersonic flow, *AIAA J*, 1978, **17**, (6), pp 579-585.
3. ARNAL, D. and DELERY, J. Shock Wave Boundary Layer Interaction, NATO, May 2004.
4. OLIVER, *et al* Assessment of Turbulent Shock-Boundary Layer Interaction Computations Using the OVERFLOW Code, School of Aeronautics and Astronautics, Purdue University, January 2007.
5. SETTLES, G.S. and DODSON, L.J. Hypersonic Shock/Boundary Layer Interaction Database: New and Corrected Data, NASA Contractor Report 177638, April 1994.
6. KUNTZ, D.W. *et al* Turbulent Boundary Layer properties downstream of the Shock-Wave/Boundary Layer interaction, *AIAA J*, May 1987, **25**, (5).
7. WILCOX, D.C. Turbulence Modeling for CFD, DCW Industries, California, USA, 1994.
8. ASMELASH, H. A. and SINGH, A. Numerical Analysis of Shock Wave Turbulent Boundary Layer Interaction over a 2D Compression Ramp, (IJAEST) *Int J Advanced Engineering sciences and Technologies*, April 2011, **5**, (2), pp 144-149.

https://doi.org/10.1017/S0001924000008253 Published online by Cambridge University Press